Deep Energy Autoencoder for Noncoherent Multicarrier MU-SIMO Systems

Thien Van Luong, Youngwook Ko, *Senior Member, IEEE,* Ngo Anh Vien, Michail Matthaiou, *Senior Member, IEEE,* and Hien Quoc Ngo, *Member, IEEE*

***Abstract*—We propose a novel deep energy autoencoder (EA) for noncoherent multicarrier multiuser single-input multiple-output (MU-SIMO) systems under fading channels. In particular, a single-user noncoherent EA-based (NC-EA) system, based on the multicarrier SIMO framework, is first proposed, where both the transmitter and receiver are represented by deep neural networks (DNNs), known as the encoder and decoder of an EA. Unlike existing systems, the decoder of the NC-EA is fed only with the energy combined from all receive antennas, while its encoder outputs a real-valued vector whose elements stand for the sub-carrier power levels. Using the NC-EA, we then develop two novel DNN structures for both uplink and downlink NC-EA multiple access (NC-EAMA) schemes, based on the multicarrier MU-SIMO framework. Note that NC-EAMA allows multiple users to share the same sub-carriers, thus enables to achieve higher performance gains than noncoherent orthogonal counterparts. By properly training, the proposed NC-EA and NC-EAMA can efficiently recover the transmitted data without any channel state information estimation. Simulation results clearly show the superiority of our schemes in terms of reliability, flexibility and complexity over baseline schemes.**

***Index Terms*—Deep learning, deep neural network, energy autoencoder, multicarrier systems, noncoherent energy detection.**

I. Introduction

Multicarrier transmission has become a key technology for numerous wireless systems due to its simple implementation and robustness against inter-symbol interference and delay spreading caused by multipath fading. Orthogonal frequency division multiplexing (OFDM) [1], which is the most popular multicarrier technique, has been included in various standards, such as Wi-Fi 802.11 and 3GPP's LTE. In general, OFDM is not only spectrally efficient, but also enables the use of low-complexity transceivers as it only needs one-tap equalizer per sub-carrier to effectively combat multipath fading effects.

Over the past years, many efforts have been made to improve the reliability and spectral efficiency (SE) of multi-carrier systems; in this context, OFDM with index modulation (OFDM-IM) [2] has recently emerged as a promising technique to replace conventional OFDM. In particular, OFDM-IM activates only a subset of sub-carriers to carry additional data bits via the indices of active sub-carriers without any extra needs of bandwidth or power. The error performance of OFDM-IM under channel state information (CSI) uncertainty was comprehensively analyzed in [3], [4] with the maximum likelihood (ML) and energy-based greedy (GD) detectors [5]. The reliability of OFDM-IM can be further enhanced by using coordinate interleaving [6], repetition [7], [8] and spreading codes [9], while its SE can be increased by relaxing the number of active sub-carriers [10]. Note that the aforementioned multicarrier schemes are based on coherent detection designs, where the receiver needs to estimate the CSI of all sub-carriers regardless of their activity. As a result, they may suffer from a high pilot signaling overhead, particularly under fast-varying fading channels. Thus, in [11], noncoherent OFDM-IM (NC-OFDM-IM), also known as a generalized version of frequency shift keying (FSK), was introduced, which uses only the active indices to convey data bits. In fact, this scheme utilizes simple unitary codewords, i.e., transmitted vectors, as it allows a fixed number of active sub-carriers to carry the same power. Yet, this design may not be optimal, especially when some of combinations of active indices are redundant. We aim to address this issue by devising an optimal codeword design for a noncoherent multicarrier (NC-MC) energy-based scheme, using deep learning (DL) tools [12].

Regarding noncoherent single-carrier transmissions, various energy-based detection (ED) schemes with nonnegative pulse amplitude modulation (PAM) have been investigated, especially in massive single-input multiple-output (SIMO) systems. For example, the performance of an ED-based massive SIMO system was analyzed in [13], which results in an optimal power allocation design. In [14], the effects of correlated Rayleigh fading on the performance of a similar system were investigated. In [15], the PAM constellations that maximize the minimum Euclidean distance (MED) between signal points were designed, where the resulting scheme can be termed as PAM-MED. This work also looked into the constellation design for two users, which iteratively uses two separate constellations in two time slots. In [16], a uniquely factorable hexagonal constellation was proposed for noncoherent SIMO systems, where the channels are assumed to remain unchanged in each two time slots. Besides, the constellation designs under different assumptions of the CSI statistics were presented in [17], while the channel gains were used for optimizing the PAM constellations in [18]. We note that most of existing

This work was supported by the Engineering and Physical Sciences Research Council under Grant EP/N509541/1. The work of M. Matthaiou was supported by the RAEng/The Leverhulme Trust Senior Research Fellowship under Grant LTSRF1718\14\2 and by a research grant from the Department for the Economy Northern Ireland under the US-Ireland R&D Partnership Programme. The work of H. Q. Ngo was supported by the UK Research and Innovation Future Leaders Fellowships under Grant MR/S017666/1.

Thien Van Luong, Ngo Anh Vien, Michail Matthaiou, and Hien Quoc Ngo are with the ECIT Institute, Queen's University Belfast, Belfast, BT3 9DT, UK, (email: {tluong01, v.ngo, m.matthaiou, hien.ngo}@qub.ac.uk).

Youngwook Ko is with the University of York, Heslington, York, YO10 5DD, UK, (email: youngwook.ko@york.ac.uk).

works have addressed the noncoherent ED-based single-carrier and single-user systems, while the NC-MC energy-based designs for multiuser SIMO (MU-SIMO) transmissions have been overlooked. Our work aims to fill this fundamental gap.

Recently, DL based on deep neural networks (DNNs) [12] has emerged as a powerful tool to address diverse problems in physical-layer wireless communications. For instance, in [19], channel estimation and signal detection of OFDM systems were performed by DNNs, while in [20] a DL-based detector, called as DeepIM, was proposed for OFDM-IM. Particularly, in [21], a novel end-to-end learning-based system was proposed, where both the transmitter and receiver are represented by DNNs, which are known as the encoder and decoder of an AE. This data-driven system enables a joint optimization of both the transmitter and receiver via training, leading to better performance than conventional block-based systems. The AE-based system was implemented under real-world environments in [22]. The AE concept was also applied to OFDM and noncoherent MU-SIMO systems in [23] and [24], respectively. Some end-to-end AE-based schemes under unknown channel models were proposed in [25], [26], which aim to eliminate the need of a differentiable channel model. Note that under fading channels, these learning-based schemes have to employ pilot transmissions to estimate the CSI for signal detection. To the best of our knowledge, none of the existing works has explored the potential of DL in the noncoherent ED-based systems.

In this paper, DL is first applied to noncoherent energy-based systems to improve the performance over current ED systems. Our main contributions are summarized as follows:

- We propose a novel deep energy autoencoder (EA) for single-user multicarrier SIMO systems, coined as NC-EA, whose transmitter and receiver are modeled as the encoder and decoder (DNNs) of an EA. Unlike existing schemes [21] which utilize complex signals, the encoder of NC-EA outputs a real-valued vector whose elements represent the sub-carrier power levels, while its decoder is fed only with the combined energy of signals from the receive antennas without any knowledge of CSI.
- Using NC-EA, we construct two novel DNN structures for both downlink and uplink NC-EA multiple access (NC-EAMA) schemes, in the multicarrier MU-SIMO framework. Note that NC-EAMA allows multiple users to access the same set of sub-carriers, thus can be considered as a type of noncoherent non-orthogonal multiple access (NC-NOMA), which is expected to achieve higher performance gains than the noncoherent energy-based orthogonal schemes, termed as NC-OMA.
- Various simulations clearly present that by properly training with simulated data, the proposed learning-based schemes can efficiently decode data without any CSI estimation, and outperform the hand-crafted baselines at reduced complexity. In this context, our schemes are very attractive for various machine-type communications (MTCs) [27] which require reliable, low latency and low complexity connectivity.

The rest of the paper is as follows: Section II presents the single-user NC-EA, while Section III introduces the uplink and downlink NC-EAMA systems. Simulation results are provided in Section IV. Finally, Section V concludes the paper.

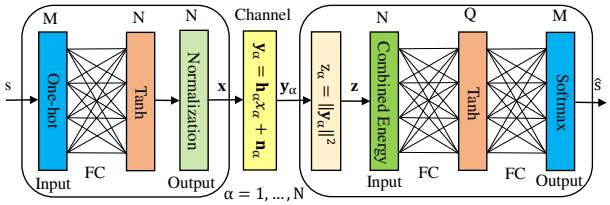

Fig. 1. Structure of the single-user NC-EA system.

Notation: Upper-case bold and lower-case bold letters present matrices and vectors, respectively; $C(n,k)$ denotes the binomial coefficient for n choose k; $\lfloor . \rfloor$ denotes the floor function; $(.)^T$ and $\|.\|$ stand for the transpose operation and the Frobenius norm, respectively. $\mathcal{CN}\left(0,\sigma^2\right)$ denotes the complex Gaussian distribution with zero mean and variance σ^2.

II. Single-User NC-EA System

A. NC-EA Structure

Consider a NC-MC SIMO system with N sub-carriers, which does not require any CSI estimation at the transmitter and the receiver. We assume that the transmitter has a single antenna, while the receiver has L antennas. Unlike current NC-MC schemes, such as NC-OFDM-IM [11], we implement both the transmitter and receiver of NC-MC by DNNs, proposing a deep energy autoencoder (EA) structure in Fig. 1, where the resulting scheme can be termed as NC-EA. Note that the proposed EA differs from the conventional AE [21] in that the decoder of the EA is fed only with the combined energy from the receive antennas, without any knowledge of CSI.

In particular, the NC-EA structure consists of the encoder and decoder neural networks, which represent the transmitter and receiver, respectively. At the transmitter, the incoming message $s \in \mathcal{S} = \{s_1, ..., s_M\}$ is mapped to an $M \times 1$ one-hot vector, which is used as an input vector of the encoder, wherein $\mathcal{S}$ is the set of all $M = 2^m$ possible messages, each having m data bits. Note that the one-hot vector $\mathbf{s}$ has a single unit entry which is indexed by s in $\mathcal{S}$, while the remaining entries are zeros. The encoder has a full-connected (FC) layer with the hyperbolic tangent (Tanh) activation function [12], whose output is given by $\mathbf{u} = \sigma_{\text{Tanh}}\left(\mathbf{W}\mathbf{s} + \mathbf{b}\right)$, where $\mathbf{W}$ and $\mathbf{b}$ are the $N \times M$ weight matrix and $N \times 1$ bias vector, respectively, and σ_{Tanh} denotes the element-wise Tanh function. Then, $\mathbf{u}$ is normalized to constrain the average transmit power over each sub-carrier to be a given constant, as follows:

$$\mathbf{x} = \frac{\sqrt{NSE_s}\mathbf{u}}{\sqrt{\sum_{i=1}^{S} \|\mathbf{u}_i\|^2}}, \tag{1}$$

where E_s is the average transmit power per sub-carrier and $\mathbf{u}_i = \sigma_{\text{Tanh}}\left(\mathbf{W}\mathbf{s}_i + \mathbf{b}\right)$ with $\mathbf{s}_i \in \Omega = \{\mathbf{s}_1, ..., \mathbf{s}_T\}$ which is a batch of S training samples (T is coined as the batch size). The set of all possible M codewords $\mathbf{x}$ can be considered as a codebook of NC-EA denoted by $\mathcal{X} = \{\mathbf{x}_1, ..., \mathbf{x}_M\}$, while the mapping from $\mathbf{s}$ to $\mathbf{x}$ can be represented by $\mathbf{x} = f_{\theta_{\text{enc}}}(\mathbf{s})$, where $\theta_{\text{enc}} = \{\mathbf{W}, \mathbf{b}\}$ denotes the parameters of the encoder.

Note that the average power normalization over an entire training batch in (1) is preferable for the energy detection of an EA than a fixed power constraint with $\mathbf{x} = \sqrt{NE_s}\mathbf{u}/\left\|\mathbf{u}\right\|$, in order to make the codewords' energies as different as possible. It is also worth noting that the codeword $\mathbf{x}$ is a real-valued vector whose entries indicate the amplitudes of sub-carrier symbols; hence, it is suitable for an energy-based decoder of NC-EA. This real-valued design also reduces the model complexity of NC-EA, which facilitates the training to converge faster, compared to the complex-valued design [21].

The received signal vector from L receive antennas, in frequency sub-carrier α, for $\alpha = 1, ..., N$, is given by

$$\mathbf{y}_\alpha = \mathbf{h}_\alpha x_\alpha + \mathbf{n}_\alpha, \tag{2}$$

where $\mathbf{y}_\alpha = \left[y_1(\alpha), ..., y_L(\alpha)\right]^T$, x_α is the α-th entry of $\mathbf{x}$, $\mathbf{h}_\alpha = \left[h_1(\alpha), ..., h_L(\alpha)\right]^T$ denotes the Rayleigh fading channel vector from the transmitter to L receive antennas with $h_l(\alpha) \sim \mathcal{CN}(0,1)$, and $\mathbf{n}_\alpha$ is the additive noise vector with $n_l(\alpha) \sim \mathcal{CN}(0, N_0)$, for $l = 1, ..., L$. We assume that the entries of $\mathbf{h}_\alpha$ and $\mathbf{n}_\alpha$ are independent and identically distributed (i.i.d.) random variables (RVs). Hence, the average signal-to-noise ratio (SNR) per sub-carrier is $\bar{\gamma} = E_s/N_0$.

As for the NC-EA decoder, the combined energy received from L receive antennas is first computed for each sub-carrier:

$$z_\alpha = \left\|\mathbf{y}_\alpha\right\|^2 = \sum_{l=1}^{L} \left|y_l(\alpha)\right|^2, \tag{3}$$

which produces the $N \times 1$ combined energy vector for all sub-carriers $\mathbf{z} = \left[z_1, ..., z_N\right]^T$. This received energy vector is then fed to the DNN of the decoder as shown in Fig. 1. In particular, the proposed decoder structure has two non-linear FC layers, in which the first FC layer has Q nodes with the Tanh activation, while the second FC layer is the output layer of M nodes with the softmax activation [12].[1] Let $\theta_{\text{dec}} = \{\mathbf{W}_i, \mathbf{b}_i\}_{i=1,2}$ be the weights and biases of the two decoder layers. The output vector of the softmax layer is mathematically expressed by

$$\hat{\mathbf{s}} = f_{\theta_{\text{dec}}}(\mathbf{z}) = \sigma_{\text{Softmax}}\left(\mathbf{W}_2 \sigma_{\text{Tanh}}\left(\mathbf{W}_1 \mathbf{z} + \mathbf{b}_1\right) + \mathbf{b}_2\right), \tag{4}$$

where σ_{Softmax} denotes the element-wise softmax function. The estimated $\hat{s}$ is determined based on the largest element of $\hat{\mathbf{s}}$.

We note that since the DNN decoder obtained via training may not be optimal for certain values of N and M, the optimal noncoherent ML may be used to improve the performance of NC-EA compared to using the DNN decoder, as follows:

$$\hat{\mathbf{x}} = \arg\min_{\mathbf{x} \in \mathcal{X}} \sum_{\alpha=1}^{N} \left[\frac{z_\alpha}{\left|x_\alpha\right|^2 + N_0} + L \ln\left(\left|x_\alpha\right|^2 + N_0\right) \right], \tag{5}$$

where we have followed the derivation of [28, Chapter 5].

It is worth noting that the NC-EA requires only the received energy for signal decoding, thus does not involve any channel estimation, which is particularly desirable for low latency and complexity communications. More importantly, our scheme provides a number of advantages over existing hand-designed schemes, such as NC-OFDM-IM [11], as follows:

- The NC-EA can send any number of data bits m for given N, while that of NC-OFDM-IM is limited to $m_0 = \lfloor \log_2 C(N, K) \rfloor$ bits, where K is the number of active sub-carriers. Hence, our scheme is not only more flexible but also is able to support higher data rates than its counterpart. For example, when $N = 4$, NC-OFDM-IM supports only $m_0 \leq 2$ bits for every $K < N$, while NC-EA supports more bits with $m = 3$ or even 4 bits.
- The NC-EA can achieve higher reliability than NC-OFDM-IM since our scheme benefits from a joint optimization of both the transmitter and the receiver through training the EA model to achieve an optimal design of codewords $\mathcal{X}$.
- The decoder of an NC-EA-based system is very simple with only one hidden layer of Q nodes. Hence, when Q is not too large, NC-EA can achieve even lower decoding complexity than NC-OFDM-IM. This will be verified in Subsection IV.B.
- The NC-EA concept can be extended to NC-NOMA, where multiple users share the same N sub-carriers for the NC-EA transmission, as will be shown in Section III. Note that this important benefit is not available in current NC-MC schemes, whose hand-designed energy-based detector is only applicable to single-user schemes.

In summary, apart from no channel estimation, the proposed NC-EA achieves higher flexibility and reliability at even lower computational complexity than existing schemes. Hence, NC-EA can be easily implemented in small and low-cost devices such as sensors. These benefits make our scheme attractive to various MTC applications [27] which demand reliable, ultra-low latency and low-complexity connectivity.

B. Training procedure of NC-EA

The proposed NC-EA model is trained to minimize the difference between the original vector $\mathbf{s}$ and its prediction $\hat{\mathbf{s}}$, using dataset collected from simulations. More precisely, the training dataset includes $\mathbf{s}$, $\mathbf{h}_\alpha$ and $\mathbf{n}_\alpha$ $(\alpha = 1, ..., N)$, in which the input one-hot vector $\mathbf{s}$ is randomly generated and fed to the encoder, then the channel and noise vectors $\mathbf{h}_\alpha$, $\mathbf{n}_\alpha$ are randomly generated and added to the output of the encoder. Then, the output of the channel layer $\mathbf{y}_\alpha$ in (2) is used for the computation of the combined energy $\mathbf{z}$ for each sub-carrier, which is fed to the DNN decoder from which $\mathbf{s}$ is recovered. We adopt the conventional mean squared error (MSE) loss function for training the NC-EA as follows:

$$\mathcal{L}(\theta) = \frac{1}{T} \sum_{i=1}^{T} \left\|\mathbf{s}_i - \hat{\mathbf{s}}_i\right\|^2, \tag{6}$$

where $\theta = \{\theta_{\text{enc}}, \theta_{\text{dec}}\}$ denotes the model parameters of NC-EA and T is the training batch size.[2] Using (6), the NC-EA

[1]The number of hidden layers is miminized based on experiments in order to make the DNN model of NC-EA perform best at a reduced complexity. Moreover, we use Tanh at both the encoder and decoder of NC-EA since this activation always offers better performance than others such as Linear, Sigmoid and Relu activations [12], as observed through our experiments.

[2]Note that based on our experiments, the MSE loss always offers comparable or better performance than the cross-entropy loss, and thus in this work we use the MSE loss only for training the proposed EA-based schemes.

model parameters are updated based on the stochastic gradient descent (SGD) algorithm as follows:

$$\theta := \theta - \eta \nabla \mathcal{L}(\theta), \tag{7}$$

where η is the learning rate which regulates how much to adjust the parameters. In this work, we adopt an advanced SGD-based update method, named as adaptive moment estimation (Adam), along with the Xavier method for initializations of weights and biases. Note that these methods are available on various off-the-shelf DL libraries, such as Tensorflow [29].

Since the NC-EA only utilizes the received energy for signal detection, its decoding performance is highly sensitive to the SNR level $\bar{\gamma}$ used for training. This means that the NC-EA model trained with a training SNR (denoted by $\bar{\gamma}_{\text{tr}}$) performs best only at the testing SNRs (denoted by $\bar{\gamma}_{\text{te}}$) that are close to $\bar{\gamma}_{\text{tr}}$, while it does not perform well at other testing SNRs that are far from $\bar{\gamma}_{\text{tr}}$. Hence, to overcome such overfitting problem, we train the NC-EA with multiple SNRs and then test the trained models with $\bar{\gamma}_{\text{te}} = \bar{\gamma}_{\text{tr}}$. As such, under varying channel variances, we need to retrain the model once $\bar{\gamma}$ changes, or store multiple pre-trained models with different $\bar{\gamma}_{\text{tr}}$. It is also necessary to accurately choose the encoder-decoder pair corresponding to each SNR before transmission. In order to reduce the training time when L is very large, i.e., massive SIMO systems, we can train NC-EA with small L, using the average received energy $\bar{z}_\alpha = \|\mathbf{y}_\alpha\|^2 / L$ rather than z_α in (3), then the trained model still works well for larger L.

Note that there are still some issues regarding training NC-EA in practice. For example, in actual systems, the channel model and statistics as described in (2) may be completely unknown, and this obviously hinders the channel gradient computation to update the transmitter. To overcome this issue, reinforcement learning [25] or generative adversarial networks [26], which has recently been used to learn the channel model of end-to-end learning-based communication systems, can be applied to NC-EA. Yet, such extensions are far beyond the scope of this work and will be part of our future work.

III. NC-EA Multiple Access Systems

Using the NC-EA, we propose two novel DNN structures for both uplink and downlink NC-EA multiple access (NC-EAMA) systems also based on multicarrier SIMO framework. Note that the proposed NC-EAMA is able to allow multiple users to share the same set of frequency sub-carriers. Then, to improve the performance, a new loss function for training NC-EAMA is designed, which ensures not only fast training convergence but also fairness performance among users.

A. Uplink NC-EAMA

The proposed structure of uplink NC-EAMA is depicted in Fig. 2, where J single-antenna users simultaneously send their data to a central access point (AP) equipped with L antennas, using the same N sub-carriers for NC-EA transmissions. Like NC-EA, the AP in uplink NC-EAMA does not require any CSI knowledge of users in the detection process. In particular, all users employ the same encoder structure as that of single-user NC-EA, which makes them have the same average transmit

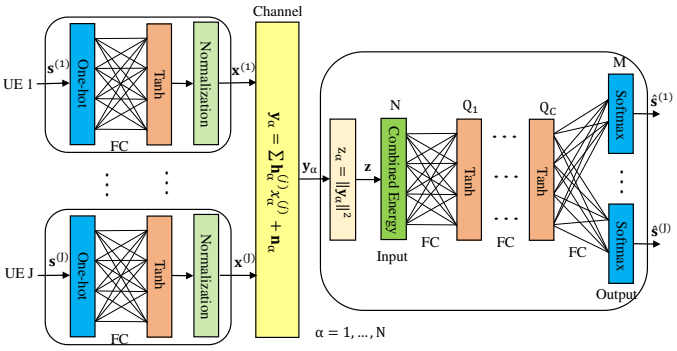

Fig. 2. Structure of the uplink NC-EAMA system.

power. We assume that $\mathbf{s}^{(j)}$ is the input vector of user j's encoder, while $\mathbf{x}^{(j)}$ is the corresponding output, i.e., $\mathbf{x}^{(j)} = f_{\theta^j_{\text{enc}}}(\mathbf{s}^{(j)})$, where θ^j_{enc} is the encoder parameters of user j. At the AP, the received signal vector at sub-carrier α is

$$\mathbf{y}_\alpha = \sum_{j=1}^{J} \mathbf{h}_\alpha^{(j)} x_\alpha^{(j)} + \mathbf{n}_\alpha, \tag{8}$$

where $\mathbf{h}_\alpha^{(j)}$ and $\mathbf{n}_\alpha$ are the $L \times 1$ channel vector from user j to the AP and the $L \times 1$ noise vector of frequency sub-carrier α, respectively, while $x_\alpha^{(j)}$ is the α-th entry of $\mathbf{x}^{(j)}$, i.e., the transmitted symbol at sub-carrier α of user j, for $j = 1, ..., J$. For the sake of simplicity of presentation, we assume that the elements of $\mathbf{h}_\alpha^{(j)}$ and $\mathbf{n}_\alpha$ have the same statistics as in Section II. Our scheme can be straightforwardly extended to the case where the channels to different users have different variances. For example, the normalization layer of each user can be scaled by a power allocation coefficient so that we can allocate more power to users with smaller channel variances.

Regarding the data decoding at the AP, similar to NC-EA, the combined energy from L receive antennas is first computed for each sub-carrier, i.e., $z_\alpha = \|\mathbf{y}_\alpha\|^2$ for $\alpha = 1, ..., N$. The resulting vector $\mathbf{z} = [z_1, ..., z_N]^T$ which collects energy from J users is used as the input of the DNN decoder. As shown in Fig. 2, the decoder structure of the AP consists of C non-linear FC hidden layers with the Tanh activation, while the output layer is divided into J independent FC sub-layers of M nodes employing the softmax activation, whose output is to determine the transmitted data of the corresponding user. Let us denote $\mathbf{W}_c$, $\mathbf{b}_c$ and Q_c as the weight, bias and number of nodes, respectively, of the c-th hidden layer of the AP decoder, whose output vector is given by $\mathbf{v}_c = \sigma_{\text{Tanh}}(\mathbf{W}_c \mathbf{v}_{c-1} + \mathbf{b}_c)$, where $\mathbf{v}_0 = \mathbf{z}$ and $c = 1, ..., C$. As a result, the output of each final sub-layer can be written by $\hat{\mathbf{s}}^{(j)} = \sigma_{\text{Softmax}}\left(\mathbf{W}_{C+1}^{(j)} \mathbf{v}_C + \mathbf{b}_{C+1}^{(j)}\right)$, where $\mathbf{W}_{C+1}^{(j)}$ and $\mathbf{b}_{C+1}^{(j)}$ are the weight and bias of the final sub-layer of user j, respectively. Finally, the transmitted message of user j is recovered according to the largest entry of $\hat{\mathbf{s}}^{(j)}$.

Note that the structure parameters of uplink NC-EAMA, such as C and Q_c $(c = 1, ..., C)$, need to be properly selected based on specific system parameters, such as N, M and J. This will be detailed for each experiment in Section IV.

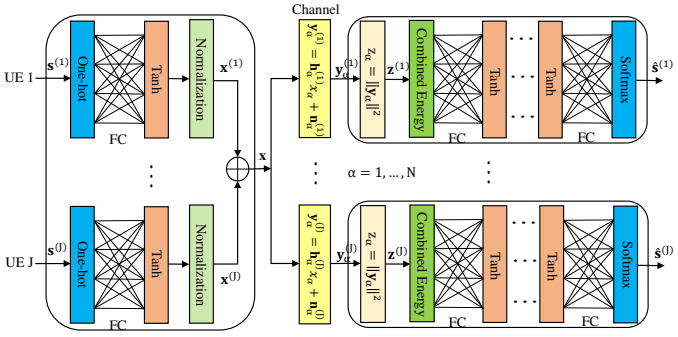

Fig. 3. Structure of the downlink NC-EAMA system.

B. Downlink NC-EAMA

The DNN structure of downlink NC-EAMA is illustrated in Fig. 3. Particularly, the AP equipped with a single antenna communicates simultaneously with J users, each of which has L antennas, applying the NC-EA technique on the same N sub-carriers. Note that the users of downlink NC-EAMA do not need any CSI knowledge to decode their data. The structure of the AP encoder consists of J sub-networks, whose structure is the same as the encoder of a single-user NC-EA. Herein, sub-network j is to encode the data of user j (denoted by the one-hot vector $\mathbf{s}^{(j)}$) into the corresponding $N \times 1$ codeword $\mathbf{x}^{(j)}$, for $j = 1, ..., J$. Then, the transmitted vector of the AP that includes the codewords of J users is determined by $\mathbf{x} = \sum_{j=1}^{J} \mathbf{x}^{(j)}$. As such, the AP allocates the same average transmit power for all users. The received signal vector of user j at sub-carrier α is written by

$$\mathbf{y}_{\alpha}^{(j)} = \mathbf{h}_{\alpha}^{(j)} x_{\alpha} + \mathbf{n}_{\alpha}^{(j)}, \tag{9}$$

where $\mathbf{h}_{\alpha}^{(j)}$ is the $L \times 1$ channel vector from the AP to the L antennas of user j, $\mathbf{n}_{\alpha}^{(j)}$ is the $L \times 1$ noise vector, both have the same statistical models as presented in the previous section, while x_{α} is the α-th element of $\mathbf{x}$.

The decoder structure of each user in downlink NC-EAMA is similar to that of single-user NC-EA, except for the fact that it now has more hidden layers to improve the decoding performance in the presence of the inter-user interference. In particular, the combined energy vector $\mathbf{z}^{(j)}$ of user j is collected as in (3), which is then fed to the corresponding DNN decoder. Denote by $\mathbf{W}_c^{(j)}$, $\mathbf{b}_c^{(j)}$ and Q_c the weight, bias and number of nodes of the c-th layer of the decoder of user j, for $c = 1, ..., C+1$, where C denotes the number of hidden layers. As a result, the output of the decoder of user j can be expressed by $\hat{\mathbf{s}}^{(j)} = \sigma_{\text{Softmax}}\left(\mathbf{W}_{C+1}^{(j)} \sigma_{\text{Tanh}}\left(...\sigma_{\text{Tanh}}\left(\mathbf{W}_1^{(j)}\mathbf{z}^{(j)} + \mathbf{b}_1^{(j)}\right)\right) + \mathbf{b}_{C+1}^{(j)}\right)$, which is used to recover the transmitted message of user j.

We now highlight some key advantages of the proposed uplink and downlink NC-EAMA as follows:

- The NC-EAMA is highly adaptive and flexible since it can be easily designed via training for any numbers of users J, frequency sub-carriers N and data streams M, as well as any type of the transmission (downlink or uplink). This flexibility is not available in existing hand-crafted schemes (e.g., NC-OFDM-IM [11], PAM-MED [15]), whose encoder and decoder must be redesigned in a complicated manner depending on the system requirements.
- As a learning scheme, the NC-EAMA allows to jointly optimize both the transmitter and receiver, which is expected to result in an optimal performance for each specific system configuration and channel condition, through properly training the models as shown in the next section.
- Compared to NC-OMA schemes, the NC-EAMA can achieve higher diversity gains since it allows multiple users to utilize all N available sub-carriers rather than just one or part of N sub-carriers as in NC-OMA. Thus, our scheme is expected to achieve higher reliability than NC-OMA, while still enjoying a low decoding complexity when the decoder requires C and Q_c to be small enough.

Note that the aforementioned benefits of the proposed NC-EAMA will be validated by simulation results in Section IV.

C. Training procedure of NC-EAMA

The uplink and downlink NC-EAMA schemes are trained offline, using dataset randomly collected by simulations, based on the known statistics of the channel and noise vectors. Unlike single-user NC-EA which simply adopts the MSE loss function for training, we design a new loss function tailored to NC-EAMA, aiming at fast training convergence to a global optimum and user fairness regarding the decoding accuracy.

In particular, for brevity, the proposed loss function is written for each single data sample, as follows:

$$\mathcal{L}(\theta) = \sum_{j=1}^{J} \mathcal{E}_j + \lambda \sum_{j=1}^{J} \left(\mathcal{E}_j - \overline{\mathcal{E}}\right)^2, \tag{10}$$

where $\mathcal{E}_j = \left\|\mathbf{s}^{(j)} - \hat{\mathbf{s}}^{(j)}\right\|^2$ is the least squared error (LSE) of user j and $\overline{\mathcal{E}} = \frac{1}{J}\sum_{j=1}^{J} \mathcal{E}_j$, while λ denotes a loss scaling factor. Note that λ is an important hyperparameter, which needs to be carefully fine-tuned while training to ensure a best performance. As seen from (10), the first term stands for the reconstruction loss, i.e., the total LSE of all users, while the second term that measures the standard deviation of the individual LSEs $\mathcal{E}_j$ is added to force them as identical as possible. Interestingly, apart from ensuring the user fairness as expected, this design enables the DNN models of NC-EAMA to quickly converge in the training process.

Similar to NC-EA, the SGD-based Adam and Xavier initialization methods are adopted for training NC-EAMA. Our proposed NC-EAMA models are trained with multiple training SNRs $\bar{\gamma}_{\text{tr}}$, and then the trained models are tested with the testing SNRs $\bar{\gamma}_{\text{te}}$ being the same as $\bar{\gamma}_{\text{tr}}$ in order to yield the best performance. The details of selecting other training parameters, such as epochs, batch size, learning rate, training and testing data sizes, and particularly the loss scaling factor λ, will be provided for various experiments in the next section.

IV. Simulation Results

We carry out extensive simulations to verify the error performance of the proposed NC-EA and uplink/downlink NC-EAMA schemes in comparison with baseline schemes.

TABLE I
NC-EA TRAINING PARAMETERS

Parameters	Values
Epoch	10^3
Batch size	128
Train size	2×10^4
Test size	10^6
Learning rate	0.001
Q	$16, 32, 64$ for $M = 4, 8, 16$

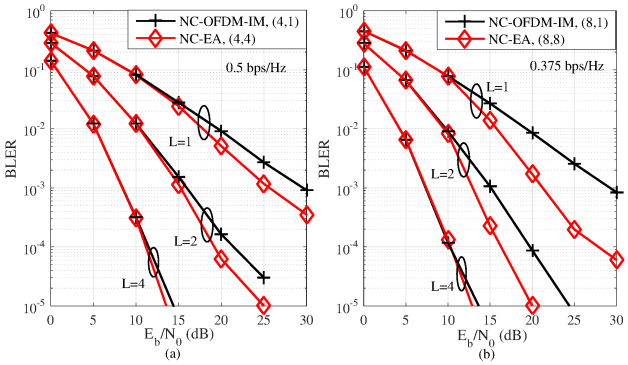

Fig. 4. BLER comparison between the proposed NC-EA and NC-OFDM-IM [11] when (a) $(N, M) = (4, 4)$ and (b) $(N, M) = (8, 8)$.

Particularly, the performance of our schemes is evaluated in terms of the block error rate (BLER) versus the average SNR per bit E_b/N_0, where $E_b = mE_s/N$ denotes the average transmit power per bit.[3] A block error event occurs when a message of m bits of each user transmitted over a block of N sub-carriers is incorrectly decoded. We also present a decoding complexity comparison at the end of this section.

A. BLER Performance of NC-EA

We consider NC-OFDM-IM [11] and PAM-MED [15] that use the noncoherent ML detector (5), as baselines of the proposed NC-EA. In particular, NC-OFDM-IM only operates at low data rates of < 1 bps/Hz, while PAM-MED operates at higher data rates of ≥ 1 bps/Hz. Note that since PAM-MED is designed for single-carrier transmission only, we independently employ it on each sub-carrier for comparison with our multicarrier scheme. Similar to NC-EA, the noncoherent ML detector of these baselines also needs to know the average SNR for data decoding. The configurations of NC-EA, NC-OFDM-IM and PAM-MED are denoted by (N, M), (N, K) and (N, D), respectively, where we recall that N is the number of sub-carriers, $M = 2^m$ with m being the size of the transmitted message of NC-EA, K is the number of active sub-carriers of NC-OFDM-IM, and D is the modulation order of PAM-MED. The training parameters of NC-EA are given in Table I.

Fig. 4 compares the BLER performance between the proposed NC-EA and NC-OFDM-IM when (a) $(N, M) = (4, 4)$ and (b) $(N, M) = (8, 8)$, and $L = 1, 2, 4$, at the data rates of 0.5 and 0.375 bps/Hz, respectively. Herein, NC-OFDM-IM activates $K = 1$ sub-carrier in both cases to achieve the same data rates as NC-EA. It is shown via Fig. 4 that our scheme outperforms the baseline, especially at high SNRs and small L. For example, in Fig. 4(b), at the BLER of 10^{-3}, NC-EA achieves 8 dB and 2 dB SNR gains over the baseline when $L = 1$ and 2, respectively. This indicates that the unitary codewords of NC-OFDM-IM are not an optimal design for every SNR level, while the proposed NC-EA can learn to return the optimal codewords for any SNR levels via training.

[3]Since the bit error rate (BER) analysis delivers the same message as the BLER analysis, for the sake of simplicity, we include the BLER results only.

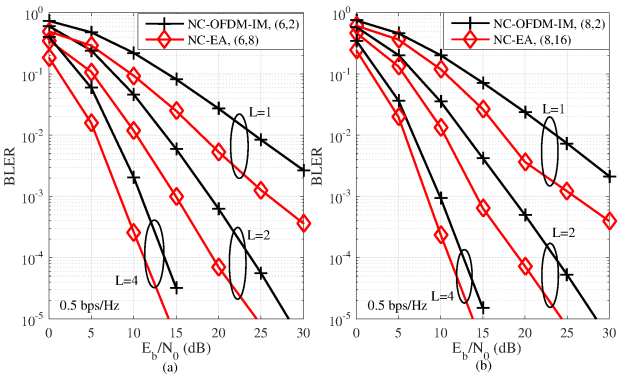

Fig. 5. BLER comparison between the proposed NC-EA and NC-OFDM-IM [11] when (a) $(N, M) = (6, 8)$ and (b) $(N, M) = (8, 16)$.

In Fig. 5, we illustrate the BLER comparison between the proposed NC-EA and NC-OFDM-IM at higher data rates with $M > N$ and $K > 1$, particularly when (a) $(N, M) = (6, 8)$ and (b) $(N, M) = (8, 16)$, and $K = 2$. Note that for given N, NC-OFDM-IM needs $K > 1$ to support higher data rate transmissions. Unlike the previous figure, it is observed from Fig. 5 that NC-EA performs much better than the baseline in whole SNR regions, even when L increases. For example, in Fig. 5(a), at a BLER of 10^{-2}, our scheme provides about 6, 3 and 2 dB SNR gains over the baseline when $L = 1, 2$ and 4, respectively. This improvement comes from the fact that when $(N, K) = (6, 2)$, the baseline has a total of $C(6, 2) = 15$ possible unitary codewords, however, it only utilizes 8 codewords to convey 3 bits, which is obviously an inefficient and sub-optimal design. By contrast, the proposed EA approach which can learn to optimize codewords appears to ideally address the drawback of the hand-designed baseline.

Fig. 6 depicts the BLER performance versus $\log_2(L)$ of the proposed NC-EA and PAM-MED at the data rates of ≥ 1 bps/Hz, when $E_b/N_0 = 10$ dB, $N = 2$, $M = 4, 8, 16$, $D = 2, 4$ and $L = 1, 2, ..., 2^9$. Note that the baseline scheme employs the PAM-MED technique with $D = 2$ and 4 on each sub-carrier to support 1 and 2 bps/Hz data rates. We point out NC-OFDM-IM is not considered since it is not able to work at more than 1 bps/Hz. The performance of NC-EA with the noncoherent ML decoder is included, besides that of the DNN decoder. As seen in Fig. 6, at 1 bps/Hz, NC-EA and PAM-MED have the same performance since when $D = 2$, PAM-MED becomes an on-off keying (OOK) scheme, which is known to be optimal in this case. At higher data rate, i.e., 2 bps/Hz, NC-EA considerably outperforms PAM-MED. For instance, at 2 bps/Hz, our scheme needs less than 32 antennas to achieve a BLER of 10^{-2}, while PAM-MED

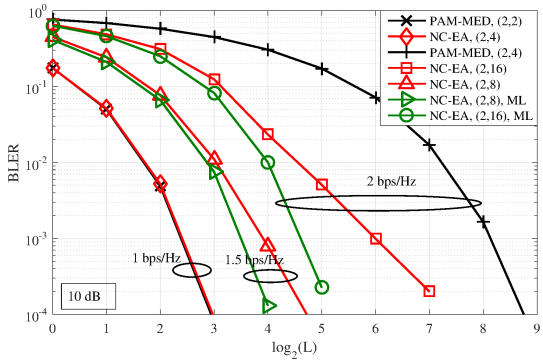

Fig. 6. BLER comparison between the proposed NC-EA and PAM-MED [15] when $E_b/N_0 = 10$ dB, $N = 2$, $M = \{4, 8, 16\}$ and $D = 2, 4$.

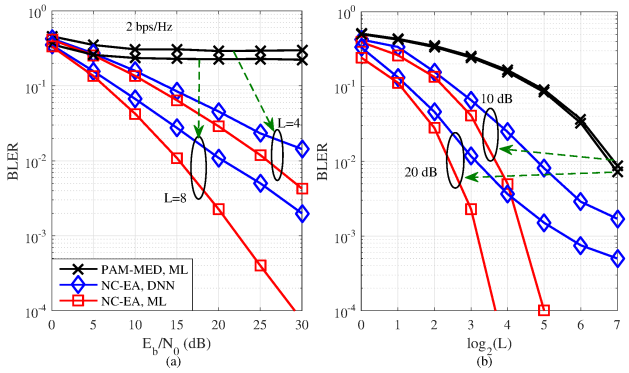

Fig. 7. BLER comparison between the single-carrier NC-EA and PAM-MED [15] when $(N, M) = (1, 4)$, (a) $L = 1, 4, 8$ and (b) $E_b/N_0 = 10$, 20 dB. The NC-EA employs ML and DNN decoders, while PAM-MED uses the ML decoder.

requires more than 128 antennas. Moreover, while the baseline is unable to support the data rate of 1.5 bps/Hz, our scheme still performs well with the BLER curve lying between the ones of 1 and 2 bps/Hz. This clearly confirms the advantage in terms of higher flexibility of NC-EA compared to hand-crafted baselines, such as NC-OFDM-IM and PAM-based schemes. Finally, in NC-EA, the optimal ML outperforms the DNN decoder as expected, especially when M and L get larger, at the cost of substantial computational complexity.

Note that the proposed NC-EA works well not only for multicarrier but also for single-carrier transmissions as shown in Fig. 7. Particularly, Fig. 7 illustrates the BLER comparison between single-carrier NC-EA and PAM-MED when $(N, M) = (1, 4)$, wherein Fig. 7(a) presents the BLER versus E_b/N_0 when $L = 1, 4, 8$, while Fig. 7(b) depicts the BLER versus $\log_2(L)$ when $E_b/N_0 = 10$ and 20 dB. Here, NC-EA employs both the DNN and noncoherent ML decoders. As seen in Fig. 7(a), while the baseline suffers from a prohibitive error floor, our scheme achieves much better BLER, which decreases with increasing the SNR. Moreover, the ML decoder significantly enhances the performance of NC-EA compared to the DNN decoder which is known to be a sub-optimal decoder. As observed in Fig. 7(b), our scheme again outperforms PAM-MED. For example, at 20 dB, NC-EA with either DNN or ML decoder only needs about 8 antennas to achieve the BLER of 10^{-2}, while the baseline requires 128 antennas.

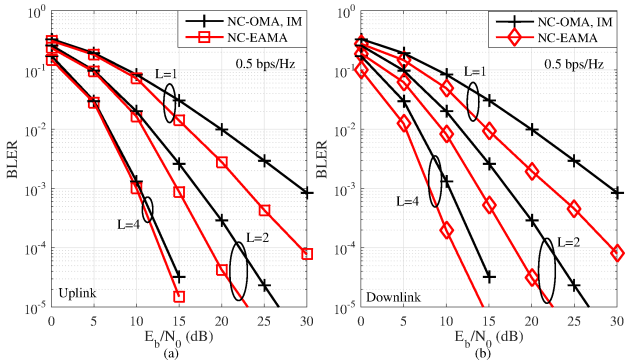

Fig. 8. BLER comparison between the (a) uplink and (b) downlink NC-EAMA, and NC-OMA with IM, when $(J, N, M) = (2, 4, 2)$ and $L = 1, 2, 4$.

B. BLER Performance of NC-EAMA

We note that NC-EAMA is the first multicarrier NC-NOMA scheme that allows multiple users to share the same set of frequency sub-carriers. Thus, it is reasonable to compare NC-EAMA with NC-OMA schemes which are based on either noncoherent IM or PAM techniques. In particular, each user in NC-OMA is evenly allocated $n = N/J$ sub-carriers to independently employ NC-OFDM-IM and PAM-MED for low and high data rate transmissions, respectively. The training parameters of NC-EAMA are the same as that of NC-EA in Table I, except for the number of hidden layers of the decoder C is fixed to 2 in all experiments, and the corresponding hidden nodes denoted by $\{Q_1, Q_2\}$ will be provided for each specific experiment. Especially, the loss scaling factor λ is empirically selected from the set of $\mathcal{F} = \{0, 1, 5, 10, 20\}$. Note from our experiments that there does not exist an optimal λ for any system parameters (J, N, M) as well as SNR levels.

Fig. 8 compares the BLER performance between the proposed (a) uplink and (b) downlink NC-EAMA, and NC-OMA with IM, when $(J, N, M) = (2, 4, 2)$ and $L = 1, 2, 4$. Herein, NC-EAMA employs $\{8, 16\}$ and $\{4, 8\}$ hidden nodes for the uplink and downlink decoders, respectively. It is shown via Fig. 8 that NC-EAMA has better BLER than NC-OMA for both uplink and downlink, especially when L is small and the SNR gets larger. For example, at the BLER of 10^{-3}, the uplink NC-EAMA achieves an SNR gain of 6.5 dB and 2.5 dB over NC-OMA when $L = 1$ and 2, respectively. The SNR gain achieved by the downlink NC-EAMA is even larger. In fact, NC-EAMA allows multiple users to simultaneously spread their transmit powers across all N sub-carriers in an optimized manner via training, achieving higher diversity gains than NC-OMA, whose users employ $n \ll N$ sub-carriers only.

Fig. 9 depicts the BLER comparison between uplink NC-EAMA and NC-OMA with PAM at higher data rate, i.e., 2 bps/Hz, when $(J, N, M) = (2, 2, 4)$ and $L = 4, 8$. The decoder of NC-EAMA has $\{16, 32\}$ hidden nodes. Note that NC-OMA with IM does not work at the considered high data rate. We can see from Fig. 9 that the BLER of the proposed scheme decreases with increasing the SNR, thus is much better than that of the baseline which incurs a very high error floor. The same observation can also be made for the downlink

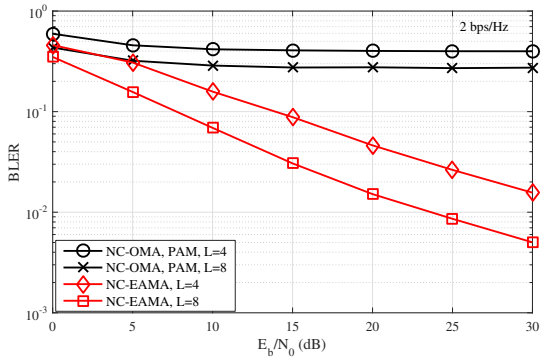

Fig. 9. BLER comparison between the uplink NC-EAMA and NC-OMA with PAM, at a data rate of 2 bps/Hz, when $(J, N, M) = (2, 2, 4)$ and $L = 4, 8$.

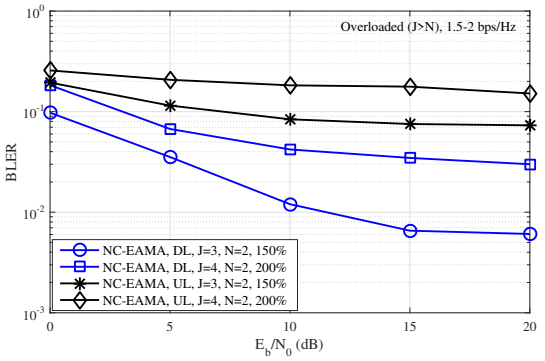

Fig. 11. BLER performance of the uplink and downlink NC-EAMA under overloaded transmissions, when $J = 3, 4$, $N = 2$, $M = 2$ and $L = 8$.

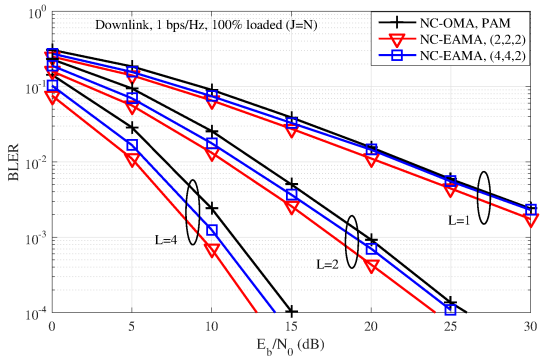

Fig. 10. BLER comparison between the downlink NC-EAMA and NC-OMA with PAM when $(J, N, M) = (2, 2, 2)$, $(4, 4, 2)$, and $L = 1, 2, 4$.

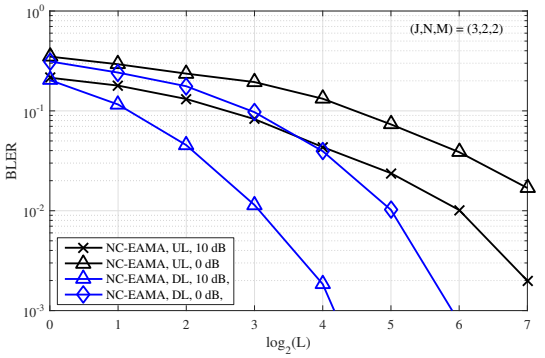

Fig. 12. BLER versus $\log_2(L)$ of the NC-EAMA under overloaded transmissions, when $(J, N, M) = (3, 2, 2)$, $E_b/N_0 = 0$ dB and 10 dB.

transmission that we omit for the sake of brevity.

In Fig. 10, we compare the performance of downlink NC-EAMA and NC-OMA with PAM when $(J, N, M) = (2, 2, 2)$, $(4, 4, 2)$, and $L = 1, 2, 4$, i.e., the system is 100% fully-loaded with $J = N$. In this case, each user of NC-OMA employs the single-carrier PAM-MED, i.e., OOK transmission, while each user of NC-EAMA has $\{4, 8\}$ hidden nodes in the decoder. It is interesting from Fig. 10 that NC-EAMA outperforms the baseline for all SNR values, in particular the performance gap between them is larger when L and N increase. This is due to the fact that more sub-carriers used for each user leads to more diversity gains achieved by NC-EAMA over NC-OAM whose users use only one sub-carrier. For uplink, we found in our experiments that NC-EAMA performs similarly to NC-OMA with PAM in the same setting.

Fig. 11 presents the BLER of uplink and downlink NC-EAMA under overloaded transmissions with $J > N$, when $J = 3, 4$, $N = 2$, $M = 2$ and $L = 8$. Herein, our schemes employ $\{16, 32\}$ and $\{8, 16\}$ hidden nodes for uplink and downlink decoders, respectively. It should be noted that hand-crafted NC-OMA schemes are unable to support overloaded transmissions, while our schemes perform relatively well under 150% and 200% overloading, especially in the downlink, as shown in Fig. 11. However, due to the severe inter-user interference when the number of users increases, while the number of sub-carriers is limited, the BLER of NC-EAMA experiences an error floor at increasing SNRs. Thus, it is essential to enable NC-EAMA to support more users under limited sub-carrier resources, while still ensuring a good performance. One solution is to increase the number of antennas L as shown in Fig. 12, where the reliability of NC-EAMA is noticeably enhanced as L gets larger, even at a small SNR of 0 dB. Also, an noncoherent ML decoder can be derived for NC-EAMA to improve its performance compared to the DNN decoder, which is considered as our future work.

C. Complexity Comparison

We investigate the detection complexity of the proposed schemes in comparison with baseline schemes using the non-coherent ML detector. In particular, we measure the runtime of successfully decoding a transmitted message of $m = \log_2(M)$ bits at the receiver by considering that all schemes are implemented on MATLAB of the same machine for fairness. Note that the trained models of our proposed schemes on Tensorflow are converted into MATLAB to compute the runtimes. Since the effect of L on the decoding complexity of all schemes is

TABLE II
RUNTIMES OF NC-EA AND IM/PAM BASELINES IN MICROSECONDS

(N, M)	NC-EA	IM [11]	PAM [15]
$(8, 8)$	8.15	4.72	N/A
$(6, 8)$	7.89	16.23	N/A
$(8, 16)$	9.62	26.85	N/A
$(1, 4)$	6.57/3.54	N/A	3.56

TABLE III
RUNTIMES OF NC-EAMA AND NC-OMA BASELINES IN MICROSECONDS

(J, N, M)	NC-EAMA	NC-OMA/IM	NC-OAM/PAM
$(2, 4, 2)$, UL	6.03	4.17	N/A
$(2, 4, 2)$, DL	7.91	4.17	N/A
$(2, 2, 4)$, UL	6.41	N/A	3.45
$(4, 4, 2)$, DL	7.74	N/A	3.28

TABLE IV
COMPLEXITY OF NONCOHERENT ML AND PROPOSED DNN DECODERS

Detection schemes	Complexity
Noncoherent ML	$\mathcal{O}(10NM) + \mathcal{O}(4NL)$
NC-EA	$\mathcal{O}(NQ + QM) + \mathcal{O}(4NL)$
Uplink NC-EAMA	$\mathcal{O}(NQ_1 + Q_1Q_2 + JQ_2M) + \mathcal{O}(4NL)$
Downlink NC-EAMA	$\mathcal{O}(NQ_1 + Q_1Q_2 + Q_2M) + \mathcal{O}(4NL)$

the same at the step of computing the combined energy, we simply adopt $L = 4$ to measure the runtimes for simplicity.

Table II compares the runtimes in microseconds (μs) between NC-EA and NC-OFDM-IM or PAM-MED baselines (abbreviated as IM/PAM on the table). Here, the system parameters (N, M) on Table II are associated with some of figures in Subsection IV.A. It is shown via Table II that NC-EA requires runtimes comparable to the baselines, which are only a few microseconds. Particularly, compared to NC-OFDM-IM, the runtime of NC-EA is larger when $N = M = 8$ and is smaller when $N < M$. This is because when $N < M$, NC-OFDM-IM needs to activate more sub-carriers, i.e., $K > 1$, which significantly increases its detection complexity compared to the case of $N = M$, i.e., $K = 1$. By contrast, the complexity of NC-EA does not increase much when N or M increases due to its simple decoder structure with a few hidden nodes as shown in Table I. This clearly confirms the benefits of our proposed scheme over NC-OFDM-IM in terms of the receiver complexity as presented in Section II. Moreover, compared to PAM-MED when $(N, M) = (1, 4)$, NC-EA with the DNN decoder requires a longer runtime, i.e., 6.57 μs. However, using the ML decoder, our scheme demands a runtime similar to the baseline with around 3.5 μs, while achieving much better BLER as in Fig. 7. Note that as N, M get larger the DNN may have lower complexity than ML decoder. For example, when $(N, M) = (16, 64)$, the runtime of the DNN decoder with 128 hidden nodes is 18 μs, which is much lower than that of the ML with 294 μs.

The runtimes of NC-EAMA and NC-OMA baselines based on either IM or PAM are depicted in Table III, where the system parameters (J, N, M) are associated with the figures in Subsection IV.B. Similar to NC-EA, both the proposed uplink and downlink NC-EAMA schemes demand slow runtimes in decoding data, which are only several microseconds. Compared to the NC-OMA baselines, NC-EAMA requires larger runtimes. This is understandable since the baselines only need to employ the single-carrier detection independently, while our scheme has to detect the signals across all sub-carriers.

Finally, to better understand the impact of system parameters, please refer to Table IV which illustrates the Big-O complexity of the noncoherent ML and proposed DNN decoders, where both downlink and uplink NC-EAMA require two hidden layers, while the ML decoder (5) is used for all baselines above. Here, the term $\mathcal{O}(4NL)$ which appears in all detection schemes refers to the complexity of computing the received energy from L receive antennas as in (3). It is shown via Table IV that the decoding complexities of the proposed schemes increase with the numbers of nodes in the hidden layers of the DNN decoders. However, when these numbers are not too large, our schemes yield comparable or even lower complexity compared with the ML decoder of the baselines as shown in the previous runtime comparison.

V. CONCLUSION

We have explored the potential of DL in noncoherent energy-based systems under fading channels, which do not involve any CSI estimation, for both single-user and multi-user transmissions under the multicarrier SIMO framework. In particular, it was shown that the proposed single-user NC-EA can provide a range of advantages over existing hand-crafted schemes, such as higher reliability, higher SE and higher flexibility with comparable or lower detection complexity. Interestingly, the NC-EA still performs well even with single-carrier transmissions. For multiuser scenarios, the proposed NC-EAMA based on the multicarrier MU-SIMO framework is also highly flexible as it can be designed to accommodate any number of users, sub-carriers, antennas and data streams, as well as any transmission directions, while current hand-crafted schemes are unable to enjoy such highly flexible designs. More importantly, developing the opportunities of the NC-NOMA scheme, NC-EAMA can achieve much higher reliability than NC-OMA counterparts, while still enjoying a low decoding complexity. We showed that the proposed NC-EAMA still works well even with overloaded transmissions, especially when the number of antennas is large enough. Hence, our proposed schemes are appropriate for MTCs which demand reliability, low latency and low complexity.

REFERENCES

[1] T. Hwang, C. Yang, G. Wu, S. Li, and G. Y. Li, "OFDM and its wireless applications: A survey," *IEEE Trans. Veh. Technol.*, vol. 58, no. 4, pp. 1673–1694, May 2009.

[2] E. Basar, U. Aygolu, E. Panayirci, and H. V. Poor, "Orthogonal frequency division multiplexing with index modulation," *IEEE Trans. Signal Process.*, vol. 61, no. 22, pp. 5536–5549, Nov. 2013.

[3] T. V. Luong and Y. Ko, "Impact of CSI uncertainty on MCIK-OFDM: Tight, closed-form symbol error probability analysis," *IEEE Trans. Veh. Technol.*, vol. 67, no. 2, pp. 1272–1279, Feb. 2018.

[4] ——, "A tight bound on BER of MCIK-OFDM with greedy detection and imperfect CSI," *IEEE Commun. Lett.*, vol. 21, no. 12, pp. 2594–2597, Dec. 2017.

[5] J. Crawford and Y. Ko, "Low complexity greedy detection method with generalized multicarrier index keying OFDM," in *Proc. IEEE PIMRC*, Aug. 2015, pp. 688–693.

[6] E. Basar, "OFDM with index modulation using coordinate interleaving," *IEEE Wireless Commun. Lett.*, vol. 4, no. 4, pp. 381–384, Aug. 2015.

[7] T. V. Luong, Y. Ko, and J. Choi, "Repeated MCIK-OFDM with enhanced transmit diversity under CSI uncertainty," *IEEE Trans. Wireless Commun.*, vol. 17, no. 6, pp. 4079–4088, June 2018.

[8] J. Choi, "Coded OFDM-IM with transmit diversity," *IEEE Trans. Commun.*, vol. 65, no. 7, pp. 3164–3171, July 2017.

[9] T. V. Luong and Y. Ko, "Spread OFDM-IM with precoding matrix and low-complexity detection designs," *IEEE Trans. Veh. Technol.*, vol. 67, no. 12, pp. 11 619–11 626, Dec. 2018.

[10] R. Fan, Y. J. Yu, and Y. L. Guan, "Generalization of orthogonal frequency division multiplexing with index modulation," *IEEE Trans. Wireless Commun.*, vol. 14, no. 10, pp. 5350–5359, Oct. 2015.

[11] J. Choi, "Noncoherent OFDM-IM and its performance analysis," *IEEE Trans. Wireless Commun.*, vol. 17, no. 1, pp. 352–360, Jan. 2018.

[12] J. Schmidhuber, "Deep learning in neural networks: An overview," *Neural Netw.*, vol. 61, pp. 85–117, 2015.

[13] M. Hammouda, S. Akin, and J. Peissig, "Performance analysis of energy-detection-based massive SIMO," in *Proc. IEEE BlackSeaCom*, May 2015, pp. 152–156.

[14] H. Xie, W. Xu, W. Xiang, B. Li, and R. Wang, "Performance of ED-based non-coherent massive SIMO systems in correlated Rayleigh fading," *IEEE Access*, vol. 7, pp. 14 058–14 069, 2019.

[15] M. Chowdhury, A. Manolakos, and A. Goldsmith, "Scaling laws for noncoherent energy-based communications in the SIMO MAC," *IEEE Trans. Inf. Theory*, vol. 62, no. 4, pp. 1980–1992, Apr. 2016.

[16] E. Leung, Z. Dong, and J. Zhang, "Uniquely factorable hexagonal constellation designs for noncoherent SIMO systems," *IEEE Trans. Veh. Technol.*, vol. 66, no. 6, pp. 5495–5501, June 2017.

[17] A. Manolakos, M. Chowdhury, and A. Goldsmith, "Energy-based modulation for noncoherent massive SIMO systems," *IEEE Trans. Wireless Commun.*, vol. 15, no. 11, pp. 7831–7846, Nov. 2016.

[18] R. K. Mallik and R. D. Murch, "Optimal ASK levels for channel magnitude based diversity reception in Rayleigh fading," *IEEE Trans. Commun.*, vol. 66, no. 9, pp. 4345–4360, Sep. 2018.

[19] H. Ye, G. Y. Li, and B. Juang, "Power of deep learning for channel estimation and signal detection in OFDM systems," *IEEE Wireless Commun. Lett.*, vol. 7, no. 1, pp. 114–117, Feb. 2018.

[20] T. V. Luong, Y. Ko, N. A. Vien, D. H. N. Nguyen, and M. Matthaiou, "Deep learning-based detector for OFDM-IM," *IEEE Wireless Commun. Lett.*, vol. 8, no. 4, pp. 1159–1162, Aug. 2019.

[21] T. O'Shea and J. Hoydis, "An introduction to deep learning for the physical layer," *IEEE Trans. Cogn. Commun. Netw.*, vol. 3, no. 4, pp. 563–575, Dec. 2017.

[22] S. Dorner, S. Cammerer, J. Hoydis, and S. T. Brink, "Deep learning based communication over the air," *IEEE J. Sel. Top. Signal Process.*, vol. 12, no. 1, pp. 132–143, Feb. 2018.

[23] A. Felix, S. Cammerer, S. Dorner, J. Hoydis, and S. T. Brink, "OFDM-autoencoder for end-to-end learning of communications systems," in *Proc. IEEE SPAWC*, June 2018, pp. 1–5.

[24] S. Xue, Y. Ma, N. Yi, and R. Tafazolli, "Unsupervised deep learning for MU-SIMO joint transmitter and noncoherent receiver design," *IEEE Wireless Commun. Lett.*, vol. 8, no. 1, pp. 177–180, Feb. 2019.

[25] F. A. Aoudia and J. Hoydis, "End-to-end learning of communications systems without a channel model," in *Proc ACSSC*, Oct. 2018, pp. 298–303.

[26] H. Ye, G. Y. Li, B. F. Juang, and K. Sivanesan, "Channel agnostic end-to-end learning based communication systems with conditional GAN," in *Proc IEEE Globecom*, Dec. 2018, pp. 1–5.

[27] C. Bockelmann *et al.*, "Massive machine-type communications in 5G: Physical and MAC-layer solutions," *IEEE Commun. Mag.*, vol. 54, no. 9, pp. 59–65, Sep. 2016.

[28] S. M. Kay, *Fundamentals Of Statistical Processing, Volume 2: Detection Theory*. Prentice-Hall, 2009.

[29] M. Abadi *et al.*, "TensorFlow: Large-scale machine learning on heterogeneous systems," 2015. [Online]. Available: https://www.tensorflow.org/

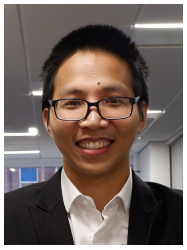

Thien Van Luong is currently a Research Fellow at University of Southampton, UK. He is also a Quantitative Analyst on financial time-series data analysis at Tenokonda Ltd., London. He obtained his Ph.D. from Queen's University Belfast, UK, in 2019, and B.S. degree from Hanoi University of Science and Technology, Vietnam, in 2015. In 2016, he was a Research Assistant with Singapore University of Technology and Design. His research interests include quantum communications, and applied machine learning in wireless signal processing.

Youngwook Ko received Ph.D. in 2006 and M.S. in 2002, in Electrical Engineering from Arizona State University, Tempe, AZ USA. He currently works for the Department of Electronic Engineering at University of York in the UK, as a senior lecturer. Prior to this, Dr Ko worked at several places. In 2007, he joined Samsung Elec. Co. as a senior research engineer. In 2008, he returned to academia as a postdoctoral fellow at the University of Alberta, Canada. He worked in the CCSR/5GiC, University of Surrey, UK, between 2010-2013 as a research fellow and then senior fellow. Between 2013-2019, Dr. Ko worked at the Queen's University Belfast, as a lecturer. He is on the Editorial Boards of the IEEE Open Journal of Vehicular Technology (OJVT) and the Elsevier Journal on Physical Communications and act as a member of the EPSRC Peer Review Associate College. His current research interests are the application of machine learning and signal processing for wireless communications and autonomous device-level communications.

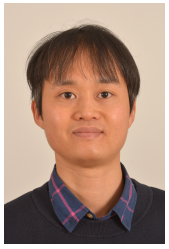

Ngo Anh Vien received the B.S. degree in computer engineering from the Hanoi University of Science and Technology, Vietnam, in 2005, and the Ph.D. degree in computer engineering from Kyung Hee University, South Korea, in 2009. He was a Postdoctoral Researcher with the National University of Singapore, from 2009 to 2011, the Ravensburg-Weingarten University of Applied Sciences, Germany, from 2011 to 2013, and the Machine Learning and Robotics Laboratory, University of Stuttgart, from 2013 to 2017. He has been a Lecturer (an Assistant Professor) with Queen's University Belfast, U.K., since 2017. His research interests include machine learning and robotics.

Michail Matthaiou (M'08–SM'13) is currently a Reader (equivalent to Associate Professor) in Multiple-Antenna Systems at Queen's University Belfast, United Kingdom. His research interests span signal processing for wireless communications, massive MIMO systems, hardware-constrained communications, mm-wave systems and deep learning for communications. Dr. Matthaiou and his coauthors received the IEEE ComSoc Leonard G. Abraham Prize in 2017. He was awarded the 2018/2019 Royal Academy of Engineering/The Leverhulme Trust Senior Research Fellowship and recently received the 2019 EURASIP Early Career Award. His team was also the Grand Winner of the 2019 Mobile World Congress Challenge. He has co-authored papers that received best paper awards at the 2018 IEEE WCSP and 2014 IEEE ICC and was an Exemplary Reviewer for IEEE COMMUNICATIONS LETTERS for 2010. He is currently the Editor-in-Chief of Elsevier Physical Communication and a Senior Editor for IEEE WIRELESS COMMUNICATIONS LETTERS.

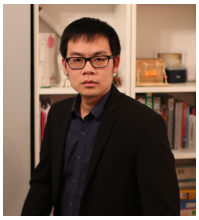

Hien Quoc Ngo is currently a Lecturer at Queen's University Belfast, UK. His main research interests include massive (large-scale) MIMO systems, cell-free massive MIMO, physical layer security, and cooperative communications. He has co-authored many research papers in wireless communications and co-authored the Cambridge University Press textbook *Fundamentals of Massive MIMO* (2016). Dr. Hien Quoc Ngo received the IEEE ComSoc Stephen O. Rice Prize in Communications Theory in 2015, the IEEE ComSoc Leonard G. Abraham Prize in 2017, and the Best PhD Award from EURASIP in 2018. He also received the IEEE Sweden VT-COM-IT Joint Chapter Best Student Journal Paper Award in 2015. He was awarded the UKRI Future Leaders Fellowship in 2019. He currently serves as an Editor for the IEEE Wireless Communications Letters, the Digital Signal Processing, the Elsevier Physical Communication, and the IEICE Transactions on Fundamentals of Electronics, Communications and Computer Sciences. He was a Guest Editor of IET Communications, and a Guest Editor of IEEE Access in 2017.